PAPER

Efficient thermal spin injection in metallic nanostructures

IOP Publishing Journal of Physics D: Applied Physics
J. Phys. D: Appl. Phys. **50** (2017) 465003 (8pp) https://doi.org/10.1088/1361-6463/aa8b5b

Efficient thermal spin injection in metallic nanostructures

Tatsuya Nomura[1], Taisei Ariki[1], Shaojie Hu[2,3] and Takashi Kimura[1,2]

[1] Department of Physics, Kyushu University, 744 Motooka, Fukuoka 819-0395, Japan
[2] Research Center for Quantum Nano-Spin Science, Kyushu University, 744 Motooka, Fukuoka 819-0395, Japan
[3] Center for Spintronics and Quantum System, State Key Laboratory for Mechanical Behavior of Materials, School of Materials Science and Engineering, Xi'an Jiaotong University, Xi'an, Shaanxi 710049, People's Republic of China

E-mail: t-kimu@phys.kyushu-u.ac.jp

Received 9 July 2016, revised 18 August 2017
Accepted for publication 8 September 2017
Published 25 October 2017

Abstract

Thermal spin injection is a unique and fascinating method for generating spin current. If magnetization can be controlled by thermal spin injection, various advantages will be provided in spintronic devices, through its wireless controllability. However, the generation efficiency of thermal spin injection is believed to be lower than that of electrical spin injection. Here, we explore a suitable ferromagnetic metal for an efficient thermal spin injection, via systematic experiments based on diffusive spin transport under temperature gradients. Since a ferromagnetic metal with strong spin splitting is expected to have a large spin-dependent Seebeck coefficient, a lateral spin valve based on CoFe electrodes has been fabricated. However, the superior thermal spin injection property has not been observed, because the CoFe electrode retained its crystalline signature—where s-like electrons dominate the transport property in the ferromagnet. To suppress the crystalline signature, we adopt a CoFeAl electrode, in which the Al impurity significantly reduces the contribution from s-like electrons. Highly efficient thermal spin injection has been demonstrated using this CoFeAl electrode. Further optimization for thermal spin injection has been demonstrated by adjusting the Co and Fe composition.

Keywords: spin injection, spin current, heat current, spin-dependent transport

(Some figures may appear in colour only in the online journal)

1. Introduction

Spin current, which is a flow of spin angular momentum, plays a central role in the operation of spin-based nano-electronic devices. The efficient manipulation of spin current is an imperative, primary issue for developing functional, energy efficient nano-spintronic devices [1–6]. Spin current is mainly generated by applying an electric field across a ferromagnetic/nonmagnetic metal interface—this process, known as electrical spin injection, was first proposed by Johnson and Silsbee over 30 years ago [7, 8]. With the development of nano-fabrication techniques, electrical spin injection has been extended to laterally configured multi-terminal ferromagnetic/nonmagnetic hybrid nanostructures [9]. In these structures, with a nonlocal spin-injection geometry, a pure spin current, which does not carry any charge current, can be created [9–12]. This pure spin current has several advantages such as the suppression of Joule heating and maximization of spin current. Although pure spin current is an attractive quantity, the preparation of independent electrodes for generating pure spin current is meanwhile indispensable. This leads to complications in device fabrication and integration.

In place of electrically-driven spin current generation, utilizing heat has recently attracted considerable attention as a new approach for controlling spin current in ferromagnetic/nonmagnetic hybrid nanostructures [13–24]. The control of the spin current using heat was also studied in a pioneering work on spin-dependent thermoelectric effects by Johnson

and Silsbee 30 years ago [8, 13]. With the development of spintronics, the unique interactions between magnetism and thermoelectricity in magnetic multi-layered or granular systems have been reported by a few groups from the fundamental view point for the heat and charge transports [15–18]. After the discovery of spin-transfer switching, spin-dependent thermoelectric effects have been paid considerable attention from the application point of view, in the emerging field of spin caloritronics. A fascinating, representative phenomenon here is the spin Seebeck effect, in which the temperature gradient across the interface between ferromagnet and nonmagnet creates a spin current [19]. The spin Seebeck effect can create spin current not only in the ferromagnetic metal but also from the ferromagnetic insulator, and opens the door to novel applications in spintronics [22]. However, recent experimental studies have pointed out the importance of ferromagnetic proximity effects in ferromagnetic/heavy metal bilayer systems [25]. In particular, since the spin Seebeck effect is always detected via inverse spin Hall effects in nonmagnetic heavy metals, the possibility of the contribution from the anomalous Nernst effect cannot be overlooked [26]. Therefore, the quantitative understanding of the spin Seebeck effect is still under consideration.

Along with the spin Seebeck effect, thermal spin injection is known as another approach to generating spin current using heat [14], [23–25]. The origin of thermal spin injection is the spin dependence of the Seebeck coefficients, while the spin Seebeck effect originates from thermally excited spin pumping [13, 14]. Therefore, this phenomenon is often called the spin-dependent Seebeck effect. The first demonstration of thermal spin injection was reported by Slachter *et al* [23]. By manipulating the heat flow due to a Joule heating in specially-developed laterally configured ferromagnetic/nonmagnetic hybrid nano-structures, they have succeeded in detecting the thermally excited spin-valve signal even at room temperature. This report was recognized as the pioneering work for thermal spin injection. However, the magnitude of the spin signal obtained was much smaller than the electrically-driven spin signals.

The thermal spin injection in a magnetic tunnel junction was also demonstrated by Walter *et al* [24]. Since the microscopic mechanism of this phenomenon is the spin dependence of the Seebeck coefficient of a tunnel junction for the ferromagnetic electrode, this is known as magneto-Seebeck tunneling or Seebeck spin tunneling effect. In [24], a laser beam was used in order to produce an efficient heat flow across the tunnel barrier, obtaining a relatively large spin-valve-like thermoelectric voltage, compared with the metallic-junction device. The Seebeck spin tunneling effect has been demonstrated in a semiconductor by using a three-terminal Hanle effect, which is a powerful technique for detecting spin accumulation in semiconductors [25]. Owing to the large resistivity of the semiconductor, the Joule heating from the electric current efficiently produced a temperature gradient, resulting in thermal spin injection. Moreover, voltage tuning of the thermally excited spin current was also demonstrated [27].

The induced thermoelectric spin voltages in the tunnel junctions were much larger than those for the metallic devices [23, 28, 29]. However, the magnitude was ten times smaller than the electrically induced signal. Moreover, because of the large interface resistance, the generated spin current was much smaller than the metallic structure. These features were considered as disadvantages from the application view point. However, thermal spin injection can be performed without the use of electricity; an innovative approach to switching the magnetization, such as wireless and/or energy harvesting operation, may be developed. Indeed, the spin transfer torque induced by thermally excited spin currents has been experimentally demonstrated in magnetic multi-layered films. Therefore, the improvement of the generation efficiency of thermally-driven spin current is an imperative and primary issue.

Recently, we have demonstrated that a CoFeAl alloy shows excellent performance in thermal spin injection, because of its favorable band structure [30]. This may open up possibilities for utilizing the thermally-driven spin current in a practical device. By performing further optimization of the materials, we may be able to demonstrate more efficient thermal spin injection, and more functional device operation. In this article, we explain a strategy for increasing thermal spin injection efficiency using a CoFe-based alloy, with reference to our systematic experiment. In addition, further possibilities for thermal spin injection will be introduced.

2. Analytical solution of thermal spin injection

To simplify the thermoelectric transport in the ferromagnetic metal system, we adopt the Mott model in diffusive metallic systems [31]. The Seebeck coefficient is strongly correlated to the band structure around the Fermi level, and, under a simple approximation in a metal, the coefficient is proportional to the energy derivative of the logarithmic density of state D at the Fermi level [31–33]. According to Mott's model, the Seebeck coefficient for a degenerate metal is simply given by the following equation:

$$S = -\frac{\pi^2}{3}\frac{k_B^2 T}{e}\frac{\partial \ln D}{\partial E}, \tag{1}$$

where k_B and e are, respectively, the Boltzman constant and the elementary charge of the electron. T and E are the temperature and the energy respectively.

Here, we focus on the experimental evaluation of the Seebeck coefficient. Because of the Seebeck effect, the temperature gradient produces the effective electric field in addition to any applied electric field. Specifically, under the gradients of the temperature T and electro-chemical potential μ, the flow of the electrons, which is the current density J, can be given by the following equation:

$$J = -\sigma(\nabla\mu/e - S\nabla T), \tag{2}$$

where σ is the electrical conductivity.

We here emphasize the remarkable difference between the electrically driven and thermally driven cases. In the electrically driven case, since the electrical conductivity is always positive, the electrons always flow in the same direction. In the thermally driven case, since the sign of the Seebeck coefficient can be either positive or negative, the direction of electron motion due to the temperature gradient depends on the material. Specifically, when the energy derivative of the density of state is positive, the Seebeck coefficient becomes negative (electron-like Fermi surface). On the other hand, when the energy derivative is negative, the Seebeck coefficient becomes positive (hole-like Fermi surface). This is a unique feature of the thermally-driven motion of the electrons.

We are now focusing on the ferromagnetic metals, in which most of the material parameters depend on the spin direction. In this case, the Seebeck coefficient should also be considered separately for up and down spins. Specifically,

$$J_\uparrow = -\sigma_\uparrow(\nabla\mu_\uparrow/e - S_\uparrow\nabla T), J_\downarrow = -\sigma_\downarrow(\nabla\mu_\downarrow/e - S_\downarrow\nabla T). \tag{3}$$

This indicates that when the Seebeck coefficient depends on the spin direction, the temperature gradient produces a spin current determined by $J_\uparrow - J_\downarrow$. This is known as thermal spin injection; it has often been called the spin-dependent Seebeck effect.

In the electrically driven case, since the signs of the electrical conductivity for up and down spins are always positive, the electrical spin polarization for the ferromagnet, which is defined by $(\sigma_\uparrow - \sigma_\downarrow)/(\sigma_\uparrow + \sigma_\downarrow)$ is always smaller than 1. This means that the generated spin current $J_\uparrow - J_\downarrow$ is less than the bias charge current $J_\uparrow + J_\downarrow$. On the other hand, for the thermal spin injection, the sign of the Seebeck coefficient can take either positive or negative value. If the signs of the Seebeck coefficient for up and down spin are opposite, a temperature gradient produces the spin current $J_\uparrow - J_\downarrow$. In this case, up-spin and down-spin currents are canceled out, leading to the reduction of the charge current $J_\uparrow + J_\downarrow$. In this situation, $(J_\uparrow - J_\downarrow)/(J_\uparrow + J_\downarrow)$ can be larger than 1. Thus, the generation efficiency of the spin current due to the thermal spin injection is significantly enhanced by the sign reversal of the Seebeck coefficient. To realize such a situation, we seek materials suitable for thermal spin injection.

According to the Stoner criterion, a ferromagnetic metal can be described by the systematic shift of the d-band center of the density of states to lower energies by an amount of energy equal to the spin splitting [34]. For conventional ferromagnets, the magnitude of the spin splitting between the up and down spins can be considered approximately as a small shift of the density of state. In this case, although the electrons for up and down spins diffuse toward the same direction with different magnitude, as shown in figures 1(a) and (b), the difference between $S_\uparrow$ and $S_\downarrow$ is very small. Therefore, the magnitude of the generated spin current diminishes. On the other hand, in a ferromagnet with strong spin splitting, the large difference in the density of state between spins produces a sign reversal of the Seebeck coefficient between the up and down spins. In such a situation, the up-spin and down-spin electrons flow in opposite directions, as shown in figures 1(c) and (d). Therefore, the generation efficiency of the spin current due to temperature gradient is significantly enhanced by the large spin-dependent Seebeck coefficient. From this point of view, we have investigated the thermal spin injection property for ferromagnetic metals with strong spin splitting.

We analytically investigate the diffusion property of the thermally-excited spin current. First, we estimate the generated spin current due to a temperature gradient in a homogeneous ferromagnet. Since there will be no spin accumulation ($\mu_\uparrow - \mu_\downarrow = 0$) in a homogeneous ferromagnet under a one-dimensional temperature gradient, the conventional Seebeck voltage with the open circuit condition ($J = 0$) can be calculated as follows.

$$\nabla\mu/e = (S_\uparrow\sigma_\uparrow + S_\downarrow\sigma_\downarrow)/(\sigma_\uparrow + \sigma_\downarrow)\nabla T = S_0\nabla T. \tag{4}$$

Here, S_0 is the effective Seebeck coefficient in the ferromagnetic systems. We then calculate the generated spin current under one dimensional temperature gradient using equation (3). Since we know the relationship between $\nabla\mu$ and ∇T, the generated spin current can be described as follows:

$$\begin{aligned} I_S &= I_\uparrow - I_\downarrow = A\nabla T(-S_0(\sigma_\uparrow - \sigma_\downarrow) + (\sigma_\uparrow S_\uparrow - \sigma_\downarrow S_\downarrow)) \\ &= (1 - P^2)A\sigma S_S\nabla T/2. \end{aligned} \tag{5}$$

Here, S_S is the spin-dependent Seebeck coefficient, defined by $S_\uparrow - S_\downarrow$. P is the electrical spin polarization, defined by $(\sigma_\uparrow - \sigma_\downarrow)/(\sigma_\uparrow + \sigma_\downarrow)$. From this equation, the spin-dependent Seebeck coefficient S_S can be seen to be the key parameter for efficient thermal spin injection.

Then, we consider the spin diffusion process in the lateral spin valve (LSV) structure under the thermal spin injection. When we introduce the temperature gradient across the ferromagnetic/nonmagnetic metal interface, the spin current given by equation (3) is generated, depending on the magnitude of the temperature gradient in the ferromagnet. The generated spin current is injected into the nonmagnet, and induces the non-equilibrium spin accumulation. This non-equilibrium spin accumulation diffuses not only into the nonmagnet but also back to the ferromagnet, similarly to the electrically generated spin current in the lateral hybrid structure. In this case, the position dependence of the spin signal due to spin accumulation is simply obtained by replacing the value of $P_F I$, where P_F is the spin polarization for the ferromagnet, in the electrical spin injection. Finally, we obtain the following equation for the spin signal due to thermal spin injection [23, 30]:

$$\Delta V_S^{2f} = \frac{P_F R_N R_F \lambda_F S_S \nabla T_F}{2R_F(R_F + R_N)(\cosh(L/\lambda_N) + \sinh(L/\lambda_N) + R_N^2\sinh(L/\lambda_N))}. \tag{6}$$

Using this equation with the spin signal under the thermal spin injection, the spin-dependent Seebeck coefficient can be estimated.

3. Comparison of thermal spin injection properties between NiFe and CoFe

We have prepared lateral spin valves consisting of two ferromagnetic wires bridged by a Cu strip, as shown in figures 2(a)

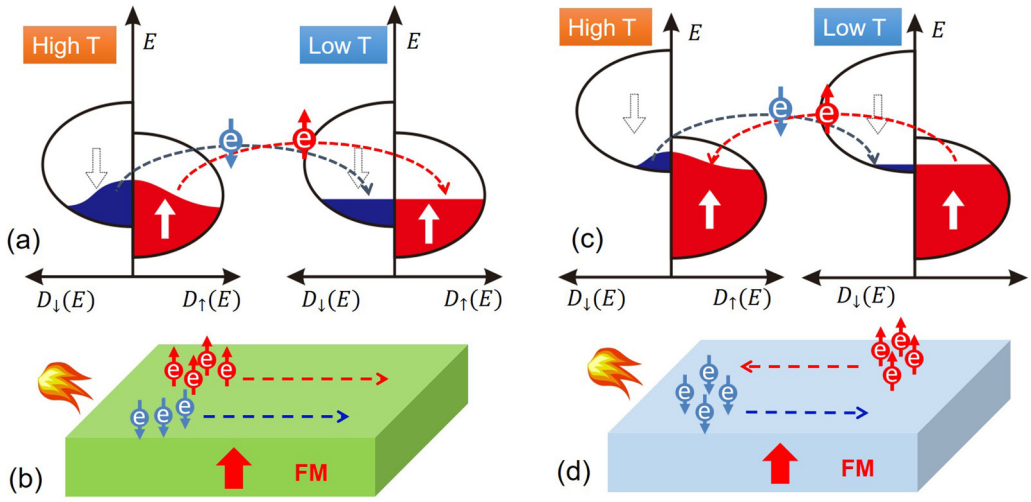

Figure 1. Schematic illustrations for the electron diffusion mechanism due to the temperature gradient. (a) Electron states at high and low temperatures and (b) electron flows due to temperature gradient for a conventional ferromagnet. (c) Electron states at high and low temperatures and (d) electron flows due to temperature gradient for a ferromagnet with strong spin splitting.

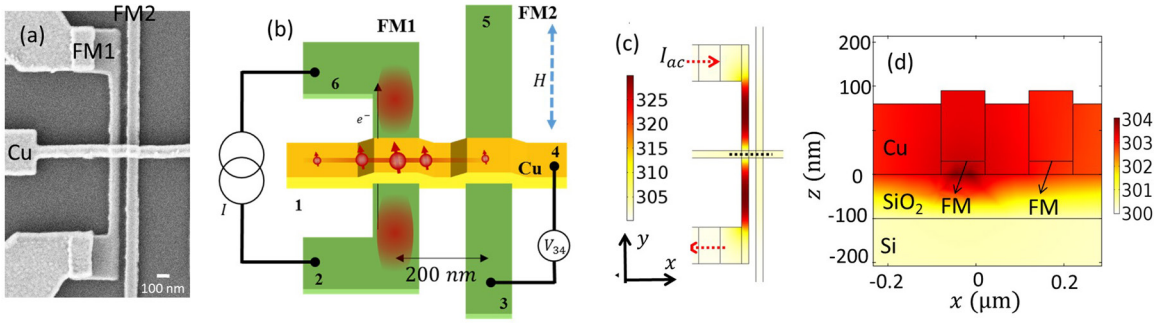

Figure 2. (a) Representative scanning electron microscope image for a fabricated lateral spin valve. (b) Schematic illustrations for the fabricated device, together with the probe configuration for the thermal spin injection. Temperature profiles under the thermal spin injection obtained by COMSOL simulation, (c) top view for the whole device and (d) cross section around the FM/Cu junctions.

and (b). Here, we adopt two representative ferromagnetic metal alloys, as ferromagnets. One is NiFe, with a relatively small magnetization, meaning that the spin splitting is not so strong. The other is CoFe, with a large saturation magnetization. According to the Stoner criterion, the large saturation magnetization is induced by the strong spin splitting. Therefore, CoFe should have stronger spin splitting than NiFe.

Here, both ferromagnetic films were deposited by conventional e-gun evaporations under the base pressure of 10^{-6} Pa. The composition of each film was measured with energy-dispersive x-ray (EDX) microscopy. For the NiFe film, Ni and Fe were 81 wt% and 19 wt% respectively. For the CoFe film, Co and Fe were 49 wt% and 51 wt% respectively. The electrical resistivities for the NiFe and CoFe are 35 $\mu\Omega$ cm and 45 $\mu\Omega$ cm respectively. The Cu strips was deposited by a Joule evaporator. Here, prior to the Cu deposition, the surfaces for the ferromagnetic wires were well cleaned by Ar ion milling with low acceleration voltage to obtain the highly transparent interface. The resistivity of Cu is 2.8 $\mu\Omega$ cm at room temperature. Here, we fixed a center–center interval between the ferromagnetic wires as 200 nm.

The thermal spin injection is performed using a local Joule heating method. By introducing a large ac current in one ferromagnetic wire, the temperature of the ferromagnetic wire significantly increases because of the Joule heating. This results in the creation of a temperature gradient across the ferromagnetic/nonmagnetic metal interface. The spin accumulation induced by the thermal spin injection is detected electrically, by another ferromagnetic wire. Here, since the temperature gradient due to the Joule heating is proportional to the current square, the induced voltage due to the thermal spin injection should be proportional to the current square. Therefore, we detect the second harmonic component of the induced voltage by using a lock-in amplifier. In this method, no contribution from the electrical spin injection will be expected, ideally, because the electric current does not flow across the interface. However, a partial current injection from the ferromagnet may be injected into the Cu around the junction, because of the low resistivity of the Cu, resulting in spin accumulation via the electrical spin injection. Indeed, we observe a spin-valve signal in the voltage component of the first harmonic frequency. However, the magnitude of the spin signal is much smaller than the conventional electrically induced nonlocal spin signal [30]. Therefore, we can exclude such contributions by the second harmonic lock-in technique.

We can estimate the temperature distribution under the local Joule heating using COMSOL simulation. As shown in figure 2(c), a temperature gradient around the interface, which

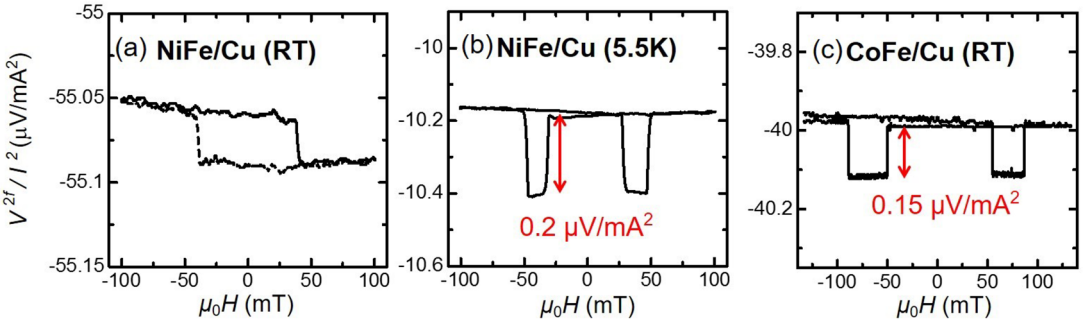

Figure 3. Experimental results for 2nd harmonic spin valve signals for NiFe/Cu LSV measured at room temperature (a) and 5.5 K (b), and for CoFe/LSV measured at room temperature (c).

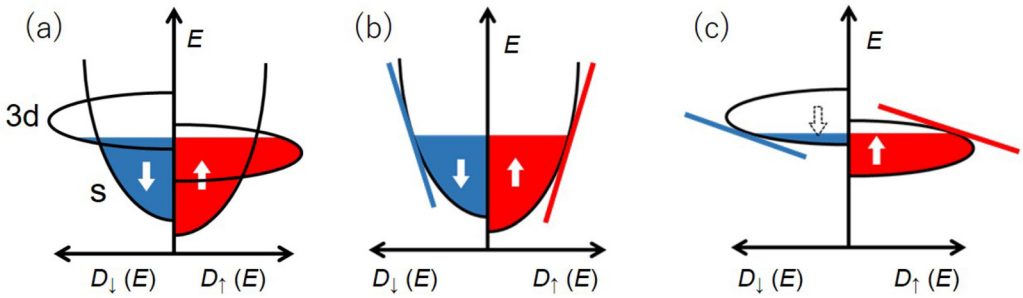

Figure 4. (a) Schematic illustration for the multi-band structure for a 3D transition metal. Density of states for s-like electron (b) and 3D electron (c).

can drive the thermal spin injection, is effectively produced by introducing a large current in the ferromagnetic injector [23, 28, 29]. From the COMSOL simulation, we can estimate the temperature gradient ∇T in the vicinity of the interface, as well as the temperature at the detecting junction, as functions of the bias ac current. We confirmed that ∇T is proportional to I^2 by COMSOL simulation.

Figures 3(a) and (c) show the 2nd harmonic spin signals under the thermal spin injection at room temperature as a function of the magnetic field for NiFe/Cu and CoFe/Cu LSVs, respectively. Here, in order to fairly compare the thermal spin injection efficiency, we take the normalized second harmonic voltage V^{2f}/I^2 as the vertical axis. This is because the temperature gradient is proportional to the Joule heating I^2, which was confirmed by COMSOL simulation. Here, we confirm that the vertical axis does not depend on the magnitude of the current amplitude below $I = 1.0$ mA. In the CoFe/Cu LSV, a typical spin-valve-like signal is clearly observed with the magnitude of 0.15 μV mA^{-2}. In the NiFe/Cu LSV, the strong asymmetric field dependence dominates the overall signal change. From the systematic study of our previous experiments, we can understand this large asymmetric signal as the anomalous Nernst effect in the ferromagnetic voltage probe [35]. When the sample is cooled to low temperature (5.5 K), the anomalous Nernst effect is strongly suppressed. On the other hand, the spin diffusion length increases with decreasing temperature [11]. Therefore, we can pick up the signal of the thermal spin injection for the NiFe/Cu LSV at low temperature. As seen in figure 3(b), we see a spin-valve-like signal, ensuring that the thermal spin injection can be achieved in the NiFe/Cu LSV. From this knowledge, by carefully observing the signal at RT, we can confirm the signature of the spin valve signal at $H \approx 25$ mT, which is caused by the magnetization reversal of the NiFe injector.

From the aforementioned results with the electrically-driven spin-diffusion property [35], we now estimate the effective Seebeck coefficient S_0 and spin-dependent Seebeck coefficient S_S for each ferromagnetic metal. From the background signal with the Seebeck coefficient for the Cu $S_{Cu} = 1.6$ μV K^{-1}, we obtain S_0 NiFe as -20.5 μV K^{-1}. This is quite consistent with the previously reported value [19, 23]. This assures the validity of COMSOL simulation. Therefore, we similarly estimate S_0 for the CoFe. The obtained value is -24.3 μV K^{-1}, which is almost the same as that for the NiFe. We then estimate the spin-dependent Seebeck coefficient from the 2nd harmonic spin signal with the calculated temperature gradient. The obtained S_S for the Permalloy and CoFe are -6.23 μV K^{-1} and -19.8 μV K^{-1} respectively. The obtained S_S for the Permalloy is reasonable value compared to the previously reported value [23]. S_S for the CoFe is larger than the NiFe, but is smaller than S_0, contrary to our expectation. Thus, the thermal spin injection efficiency is not so high, even using the CoFe alloy with strong spin splitting.

To find out the reason that S_S for our CoFe is smaller than S_0, we consider the electron state in the CoFe film. As schematically illustrated in figure 4, in 3D transition metals, the conduction electrons can be divided into two major categories [36]. One is the 3D electron, which is the basis of ferro-magnetism. As schematically shown in figure 4(c), we expect a large spin-dependent Seebeck coefficient based on the 3D band structure. The other one is the s-like electron. The spin-dependent Seebeck coefficient for s-like electrons is relatively small, because of the small difference between the up-spin and down-spin band structures, as schematically

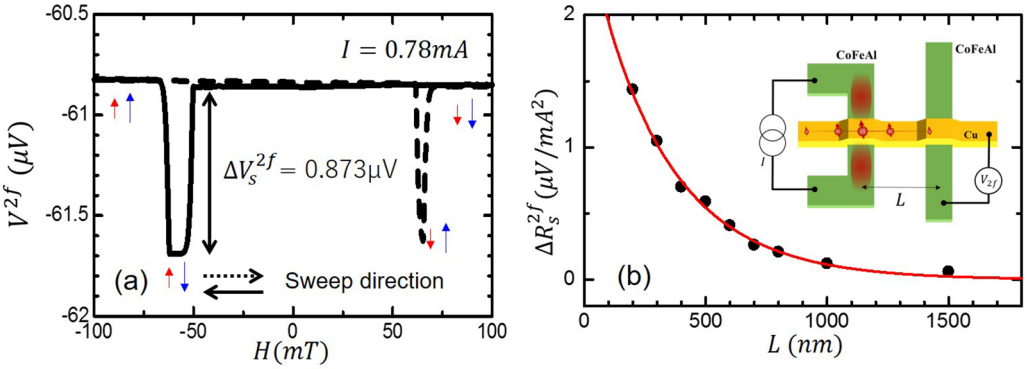

Figure 5. (a) 2nd harmonic spin valve signals for CoFeAl/Cu LSV measured at room temperature. (b) Position dependence of the 2nd harmonic spin valve signals. The red line is the fitting curve based on equation (6).

shown in figure 4(b). In the crystalline structure, owing to their long mean free path and small effective mass, the s-like electrons dominate the conduction in the ferromagnetic metal. Thus, the spin-dependent Seebeck coefficient in the CoFe becomes small, although the 3D electrons have the ideal spin-dependent band structure.

4. Efficient thermal spin injection based on CoFeAl

From the above considerations, when the contribution from the s-like electrons can be suppressed, we may exploit the ideal signature of the 3D electrons. It is well known that the mean free path for the electrons can be reduced by adding impurities, because of the resulting strong randomness of the crystalline structure. Particularly in amorphous or dirty metallic structures, the contribution of the s-electrons is significantly reduced because of their extremely short mean free path [37]. In this situation, since the number of 3D electrons is much larger than the number of s-electrons, the signature of the 3D electrons becomes visible. To realize such amorphous-like CoFe structures, we added a small amount of Al, which is one of the representative light elements. In this case, we expect a large spin-dependent Seebeck effect in CoFeAl because the Al impurities reduce the mean free path for the s-like electrons significantly.

To demonstrate the enhancement of the thermal spin-injection efficiency, we have fabricated the source of CoFeAl using an arc furnace, and deposited a CoFeAl film using an electron-beam evaporator [30]. The composition of each metal in the deposited film, evaluated using EDX, were Co 48 wt%, Fe 48 wt% and Al 4 wt% . The CoFeAl/Cu LSV was fabricated by a two-step lift-off method, similarly to the conventional LSV. We used the same device geometries, such as width and interval, as those in the previous LSV. Thermal spin signal has been measured by the 2nd harmonic detection technique of the nonlocal spin signal similarly to the previous measurements. As seen in figure 5(a), a clear spin-valve-like signal with the magnitude of 0.873 μV has been observed. The signal obtained is ten times larger than that for the CoFe/Cu LSV, implying highly efficient thermal spin injection. Using the COMSOL simulation together with the parameters from the electrical spin injection experiments, S_0 and S_S can be estimated as -22.0 μV K^{-1} and -72.1 μV K^{-1}. Also, by using the definitions for S_0 and S_S , $S_\uparrow$ and $S_\downarrow$ can be calculated as -35.7 μV K^{-1} and 36.4 μV K^{-1}. The sign difference between $S_\uparrow$ and $S_\downarrow$ is clear evidence that CoFeAl is an excellent material for thermal spin injection [30].

Here, we emphasize that the temperature of the Cu wire is not so high under the thermal spin injection. From the background signal of the second harmonic signal, the temperature change at the detection junction ΔT can be estimated to be approximately 3 K. This is because the Cu wire has a large heat conductivity and heat capacity. We can also roughly evaluate the influence of the heating effect on the Cu wire from the interval dependence of the thermal spin signal. Since the spin relaxation increases with the temperature, the spin diffusion length for the Cu should decrease at higher temperature. However, as can be seen in figure 5(b), we have confirmed that the spin diffusion length for the Cu wire is 500 nm $\pm$50 nm, which is the same as that at room temperature. These facts strongly support the validity of our analysis based on the COMSOL simulation.

For more clear evidence of the excellent performance of the CoFeAl sample, we fabricated a lateral spin valve consisting of CoFeAl and NiFe wires bridged by a Cu strip as shown in figure 6(a) [38]. In this device, we measured the 2nd harmonic spin signals in two probe configurations. One—configuration A—used NiFe as thermal spin injector and the CoFeAl as spin detector; the other—configuration B—used CoFeAl as thermal spin injector and NiFe as spin detector, as schematically shown in the insets for figure 6(b) and (c). As seen in figures 6(b) and (c), the significant difference between two signals has been observed in the thermal spin signal. In configuration A, the signal is dominated by the anomalous Nernst effect of the CoFeAl wire and a tiny spin-valve-like signal can be confirmed. This is because the poor thermal spin-dependent Seebeck coefficient for the NiFe strip. On the other hand, in configuration B, a clear spin-valve signal has been observed, because of the excellent performance of the CoFeAl. This is further evidence that the CoFeAl has a large spin-dependent Seebeck coefficient.

Thus, the strategy based on the Stoner criterion seems to work very well for efficient thermal spin injection. For further optimization of the spin-dependent Seebeck coefficient, we investigated the composition dependence of the thermal spin injection. Here, we prepared several CoFeAl alloys with

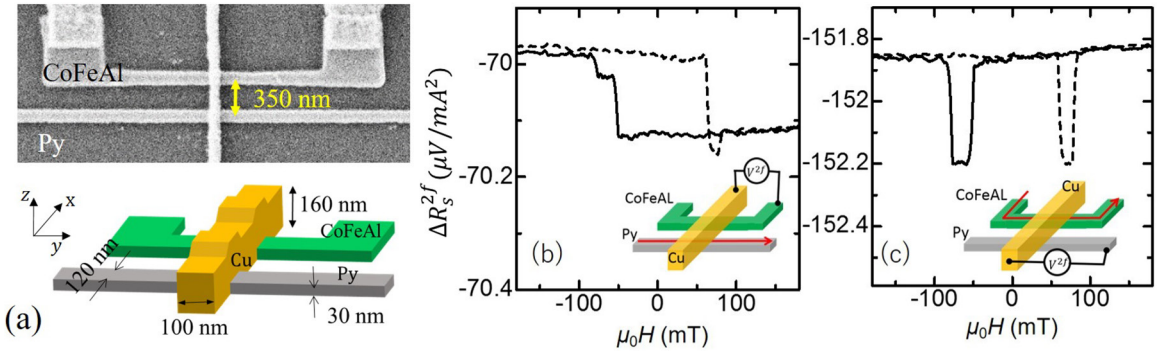

Figure 6. (a) Scacnning electron microscope image of the fabricated CoFeAl/Cu/NiFe LSV together with its schematic illustration. (b) 2nd harmonic spin valve signal for NiFe injector and CoFeAl detector and (c) that for CoFeAl injector and NiFe detector measured at room temperature.

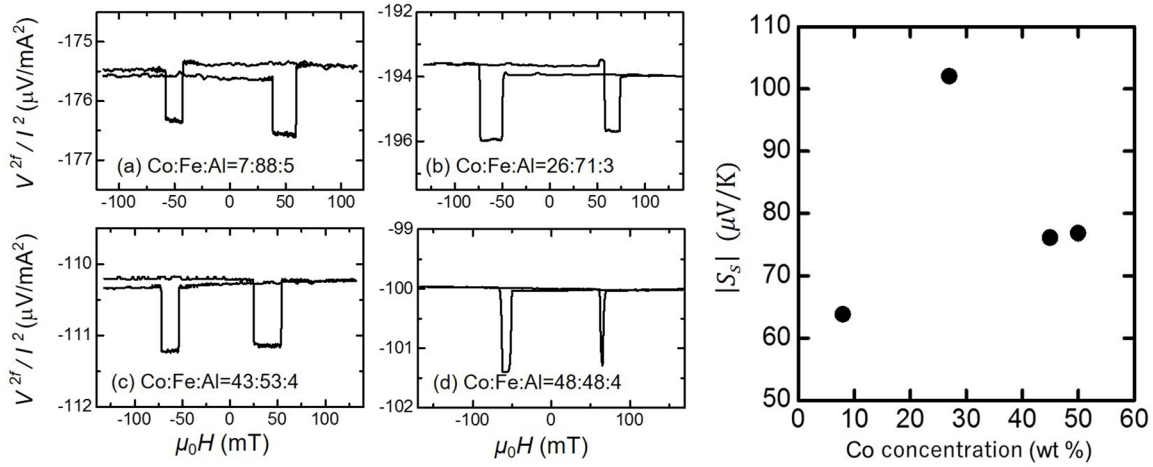

Figure 7. Room temperature 2nd harmonic spin valve signals for various CoFeAl alloy with different compositions. (a) Co 7 wt%, Fe 88 wt% and Al 5 wt%. (b) Co 26 wt%, Fe 71 wt% and Al 3 wt%. (c) Co 43 wt%, Fe 53 wt% and Al 4 wt%. (d) Co 48 wt%, Fe 48 wt% and Al 4 wt%. (e) Spin-dependent Seebeck coefficient as a function of Co composition in CoFeAl alloy.

different composition. We performed similar lateral spin-valve experiments under thermal spin injections. Figure 7(a) shows the second harmonic signal under the thermal spin injections for various CoFeAl alloys. We can confirm that the magnitude of the spin-valve-like signal changes systematically with the composition. By performing the aforementioned analysis, we estimated the spin-dependent Seebeck coefficient S_S for each alloy. Figure 7(b) shows the summary for the the spin-dependent Seebeck coefficient S_S as a function of the Co composition. S_S takes its maximum value at the composition of Co 43 wt%, Fe 53 wt% and Al 4 wt%. So, when the composition of Co is too rich, the thermal spin injection efficiency decreases. These features resemble Slater–Pauling behavior [38], suggesting a link between the two effects. However, our experiments are still very rough, and we may have to consider other mechanisms for the large spin-dependent Seebeck coefficient. For example, it was reported that the Heusler compound was partially formed in the evaporated CoFeAl film [39]. Since the energy derivative of the density of state in the Heusler compound is known to be very large, a large Seebeck coefficient will be produced. Thus, further systematic study is needed in order to conclude this matter.

5. Conclusion

We have investigated the thermal spin injection properties for various ferromagnetic metal alloys, using lateral spin valve structures. CoFe-based alloy is found to have a large spin-dependent Seebeck coefficient, which produces excellent thermal spin injection. This property can be qualitatively understood through the combination of the Mott model and Stoner criterion. We have pointed out that a small amount of Al impurity is a key to significantly increasing the spin-dependent Seebeck coefficient. We have also demonstrated that further optimization is possible by adjusting the Co and Fe compositions.

Acknowledgments

This work is partially supported by Grant-in-Aid for Scientific Research on Innovative Areas, 'Nano Spin Conversion Science' (26103002) and that for Scientific Research (S) (25220605).

References

[1] Wolf S *et al* 2001 *Science* **294** 1488–95
[2] Chappert C 2007 *Nat. Mater.* **6** 813–23
[3] Zutic I, Fabian J and Sarma S D 2004 *Rev. Mod. Phys.* **76** 323–410
[4] Maekawa S 2006 *Concepts in Spin Electronics* (Oxford: Oxford University Press)
[5] Maekawa S, Valenzuela S O V, Saitoh E and Kimura T 2012 *Spin Current* (Oxford: Oxford University Press)
[6] Tsymbal E Y and Zutic I 2011 *Spin Transport and Magnetism* (Boca Raton, FL: CRC Press)
[7] Johnson M and Silsbee R H 1985 *Phys. Rev. Lett.* **55** 1790
[8] Hu C-M 2016 *Phys. Can.* **72** 76
[9] Jedema F J, Filip T and van Wees B J 2001 *Nature* **410** 345
[10] Valenzuela S O 2009 *Int. J. Mod. Phys.* B **23** 2413
[11] Kimura T and Otani Y 2007 *J. Phys.: Condens. Matter* **19** 165216
Bakaul S, Hu S and Kimura T 2013 *Appl. Phys.* A **111** 355–60
[12] Hoffmann A 2007 *Phys. Status Solidi* c **4** 4236
[13] Johnson M and Silsbee R 1987 *Phys. Rev.* B **35** 4959
[14] Bauer G E W, Saitoh E and van Wees B J 2012 *Nat. Mater.* **11** 391–9
[15] Shi J, Pettit K, Kita E, Parkin S S P, Nakatani R and Salamon M B 1996 *Phys. Rev.* B **54** 15273
[16] Jaime M, Salamon M B, Pettit K, Rubinstein M, Treece R E, Horwitz J S and Chrisey D B 1996 *Appl. Phys. Lett.* **68** 1576
[17] Sun Y, Salamon M B, Lee M and Rosenbaum T F 2003 *Appl. Phys. Lett.* **82** 1440
[18] Gravier L, Serrano-Guisan S, Reuse F and Ansermet J P 2006 *Phys. Rev.* B **73** 024419
[19] Uchida K *et al* 2008 *Nature* **455** 778–81
[20] Scharf B, Matos-Abiague A, Zutic I and Fabian J 2012 *Phys. Rev.* B **85** 085208
[21] Le Breton J-C, Sharma S, Saito H, Yuasa S and Jansen R 2011 *Nature* **475** 82–5
[22] Uchida K *et al* 2010 *Nat. Mater.* **9** 894
[23] Slachter A, Bakker F L, Adam J-P and van Wees B J 2010 *Nat. Phys.* **6** 879–82
[24] Walter M *et al* 2011 *Nat. Mater.* **10** 742–6
[25] Qu D, Huang S Y, Miao B F, Huang S X and Chien C L 2014 *Phys. Rev.* B **89** 140407
[26] Jeon K-R, Min B-C, Spiesser A, Saito H, Shin S-C, Yuasa S and Jansen R 2014 *Nat. Mater.* **13** 360
[27] Erekhinsky M, Casanova F, Schuller I K and Sharoni A 2012 *Appl. Phys. Lett.* **100** 212401
[28] Bakaul S R, Hu S and Kimura T 2013 *Phys. Rev.* B **88** 184407
[29] Hu S, Itoh H and Kimura T 2014 *NPG Asia Mater* **6** e127
Hu S and Kimura T 2014 *Phys. Rev.* B **90** 134412
[30] Mott N F and Davis E A 1979 *Low-Dimensional Thermoelectricity* (Oxford: Clarendon) p 52
[31] Heremans J P 2005 *Acta Phys. Pol.* A **108** 609
[32] Pichard C R, Tellier C R and Tosser A J 1980 *J. Phys.: F Met. Phys.* **10** 2009–14
[33] Stoner E C 1938 *Math. Phys. Sci.* **165** 372
[34] Hu S and Kimura T 2013 *Phys. Rev.* B **87** 014424
[35] Ksendov Y M 1979 *Phys. Status Solidi* b **93** 415
[36] Mooij H 1973 *Phys. Status Solidi* a **17** 521–30
[37] Hu S *et al* 2017 *Phys. Rev.* B **95** 100403
[38] Stoner E C 1933 *Phil. Mag.* **15** 1018
Slater J C 1937 *J. Appl. Phys.* **8** 385
[39] Bridoux G, Costache M V, Van de Vondel J, Neumann I and Valenzuela S O 2011 *Appl. Phys. Lett.* **99** 102107